

Photolithography experiments using forced Rayleigh scattering

M. D. Levenson

Citation: *Journal of Applied Physics* **54**, 4305 (1983); doi: 10.1063/1.332665

View online: <http://dx.doi.org/10.1063/1.332665>

View Table of Contents: <http://scitation.aip.org/content/aip/journal/jap/54/8?ver=pdfcov>

Published by the [AIP Publishing](#)

Articles you may be interested in

[Study of thermal transport in nanoparticle suspensions using forced Rayleigh scattering](#)

J. Appl. Phys. **100**, 094310 (2006); 10.1063/1.2360378

[Measurement of mass diffusion coefficients using nonexponential forced Rayleigh scattering signals](#)

J. Chem. Phys. **109**, 267 (1998); 10.1063/1.476560

[Thermodiffusion in polymer solutions as observed by forced Rayleigh scattering](#)

J. Chem. Phys. **98**, 660 (1993); 10.1063/1.464610

[Measurement of the thermal diffusivity of liquids by the forced Rayleigh scattering method: Theory and experiment](#)

Rev. Sci. Instrum. **59**, 1156 (1988); 10.1063/1.1139743

[Dye diffusion in swollen gels by forced Rayleigh scattering](#)

J. Appl. Phys. **53**, 6513 (1982); 10.1063/1.330077

The advertisement features a dark blue background with a glowing blue light effect. On the left, there is a stylized image of a film strip with a purple and yellow textured surface. The text is centered and reads: 'Not all AFMs are created equal' in orange, 'Asylum Research Cypher™ AFMs' in white, and 'There's no other AFM like Cypher' in orange. At the bottom left, the website 'www.AsylumResearch.com/NoOtherAFMLikeIt' is written in white. At the bottom right, the Oxford Instruments logo is shown, consisting of the word 'OXFORD' above 'INSTRUMENTS' in a white box, with the tagline 'The Business of Science®' below it.

Photolithography experiments using forced Rayleigh scattering

M. D. Levenson

IBM Research Laboratory, San Jose, California 95193

(Received 31 January 1983; accepted for publication 13 April 1983)

Phase conjugate wavefront generation by degenerate four-wave mixing has been used to project images with spatial resolution greater than 500 line pairs per millimeter. The nonlinear medium, a solution of rhodamine 6G in acetone, produced the images by forced Rayleigh scattering. These images were bright enough to expose photoresist in 30 sec and their quality was adequate for fine-line lithography and consistent with theoretical expectations.

PACS numbers: 42.65.Cq, 42.30. — d, 85.40.Mt

INTRODUCTION

In previous experiments, we showed that the images projected by phase conjugate wavefront generation by degenerate four-wave mixing have resolution sufficient for fine-line lithography.^{1,2} Those experiments employed cw ion lasers with high quality TEM₀₀ output beams but relatively low average power. The conjugator materials available in large optical quality samples could not project bright images in configurations compatible with high resolution when pumped with such lasers. Literally hours were required to project each 1-cm² chip image. Other experiments showed that forced Rayleigh scattering could produce conjugate beams with reflection efficiency up to 300% at the pump intensity levels characteristic of unfocused rare gas halide laser beams.^{3,4} We found that reflection efficiencies of several percent could be obtained in a geometry theoretically consistent with high resolution.⁵

The purpose of the experiments reported here was to verify that images of sufficient quality and brightness for line lithography could, in fact, be projected by forced Rayleigh scattering. The light source employed was the 1-W average power third harmonic of an available Nd:YAG laser. Average power levels two orders of magnitude greater are possible with specially engineered ultraviolet sources. The conjugator medium was an absorbing liquid solution of rhodamine 6G dissolved in acetone. The geometry as shown in Fig. 1 was very similar to that employed in the cw laser experiments.² We found image resolution in one dimension up to 800 lines per millimeter and verified this by scanning electron microscope inspection of developed photoresist films. Image brightness was sufficient to properly expose 1-cm² images in 2–12 min. The high peak powers characteristic of our pulsed laser source led to various difficulties, including damage to the mask and beam splitter cube, but no unexpected degradation of the image was detected. With higher pump power and more refined optical engineering, lithographic exposure by conjugate wavefront generation could be made practical.

In the second section of this paper, we describe the design of our prototype exposure system and the considerations that lead to the final design. The third section describes the operation of this system along with the photoresist coating and developing procedures. The fourth section discusses our experimental results and difficulties. The final section delineates our proposals for a practical production camera.

APPARATUS

The laser in our experimental image projection system was a Quanta-Ray DCR-1A Nd:YAG unstable resonator system equipped with “filled-in” beam optics and an electronically controlled Q-switch. This laser had a cavity length of 120 cm and operated with several axial modes but gave adequate coherence length when the electronically controlled Q-switch was used without an intracavity etalon. The amplified output was converted to the third harmonic at 355 nm in the standard way with two KD*P crystals, and the horizontally polarized third harmonic beam was separated from the fundamental and second harmonic with two equilateral prisms. The average power of the third harmonic at the prisms was typically 1.2 W at 10 pps; a 10-ns pulse width implied a peak power of 12 MW.

While the third harmonic beam did not have the dark hole characteristic of diffraction coupled resonators, it did develop an intense central spot downstream which was capable of damaging optics. To smooth the beam profile, the third harmonic was focused with a 50-cm focal length lens into an evacuated cell containing a 150- μ m-diam tungsten carbide aperture. The transmitted portion (typically 60%) was recollimated by a second 50-cm focal length lens and

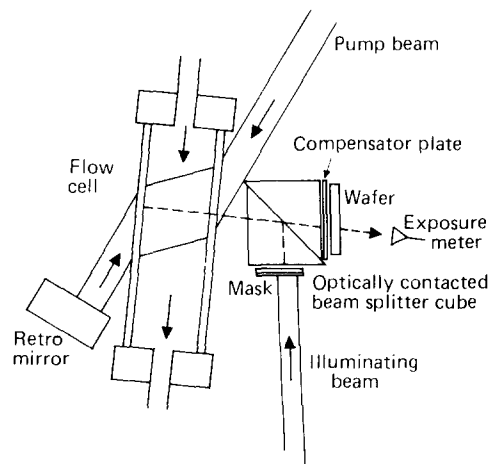


FIG. 1. Schematic of the forced Rayleigh scattering projection lithography apparatus. The faces of the beam splitter cube were 20 mm square, and the compensator plate was roughly 0.6 mm in thickness. Otherwise, the figure is roughly to scale. Not shown are the laser source and optics necessary to reshape and direct the beams.

split into pump and illuminating beams. The pump was compressed in the horizontal plane with two 45° prisms oriented away from the angle of minimum deviation. The pump beam was reflected into the conjugator medium, as shown in Fig. 1, entering at about Brewster's angle. The illuminating beam was directed onto the mask and hence through a beam splitter onto the conjugator cell. At the cell, the pump beam was rectangular in cross section with dimensions 3.3 and 3.9 mm in the horizontal and vertical directions and had average power of 280 mW. At the mask the illuminating beam dimensions were 7.5×4.0 mm with average power of 58 mW.

The pump beam traversed the 2-cm-thick conjugator cell at an angle of roughly 35° from the normal and was reflected back through the cell by a retro-mirror mounted on an NRC precision differential mount. The direction of the retroreflected pump beam was exceedingly critical; a deviation of a few microradians in the horizontal plane reduced the phase conjugate reflectivity essentially to zero. The Brewster's angle pump geometry was chosen over a 90° geometry in which the pump and object beams would enter through different faces of a rectangular conjugator cell because of the greater toleration of the Brewster's angle geometry for pump beam misalignment.

The mask consisted of a pattern of apertures etched into 700 Å of bright chrome deposited on a UV grade quartz substrate. Similar chrome-on-glass films without etched apertures had shown damage thresholds well above the intensity levels produced in these experiments. Nevertheless, mask damage continued to be a serious issue throughout the program. The diffraction pattern produced by the mask was directed into a quartz beam splitter cube. Since the open area of the mask was at most a few percent of the total area, and since the widest apertures were 10 μ or so across, the power and intensity at the reflective beam splitter surface were much lower than at the mask. Even so, we found that the nominally transparent cements used to hold the two prisms forming the beam splitter tended to damage.

Damage to the beam splitter could be avoided by eliminating the optical cement and substituting an optically contacted beam splitter for the cemented cube. The technology of optical contacting does not permit precision assembly, and the optically contacted beam splitters that we were able to obtain were hardly cubes. The two prisms that had been contacted along their hypotenuses were found to have been translated along the diagonal making the beam splitter more a rectangular parallelepiped than a cube (see Fig. 1). This asymmetry of the beam splitter is serious, because wavefront conjugation cancels all optical aberrations *except* those introduced by the beam splitter. The different ray paths for object waves reflected by the beam splitter and conjugate image waves transmitted through the partially reflecting surface introduces an uncompensated spherical aberration.

Figure 2 shows how this aberration arises. The diagram at the top shows the input surface of the beam splitter cube and the rays emanating from an object point. The phase conjugator reverses these rays to form the image, but if the actual location of the output face of the beam splitter is as shown by the lower diagram, the Snell's law refraction at the surface

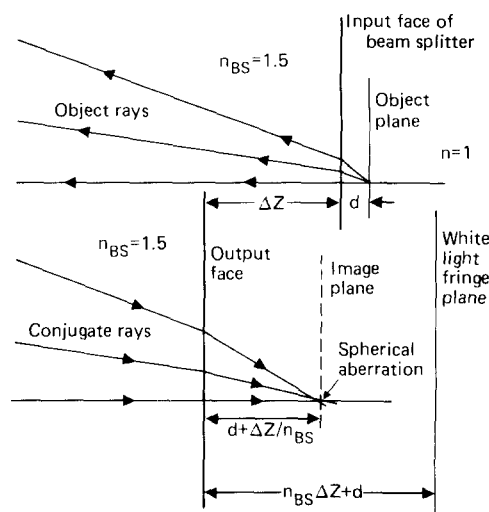


FIG. 2. Ray traces showing the effects of asymmetry in the beam splitter. Rays originating at an object on the mask are shown at top. The effect of the partially reflecting surface of the beam splitter has been omitted from the drawing, and the only influence of the beam splitter is to refract the rays at the surface. Conjugate wavefront generation produces rays inside the beam splitter that propagate along paths near the output face that are identical to those near the input face. Displacement of the output face from a position symmetric with the input introduces unwanted optical effects. The displacement ΔZ shifts the plane of best focus and the white light fringe plane used as a focusing reference, as well as creating spherical aberration and magnification error.

prevents the image rays converging to a point. In addition, the image point location is translated from the phase conjugate point, thereby introducing a magnification error. The plane of white light fringes (which we have used as a reference plane to facilitate focusing) is also deviated from the image plane. Ray tracing calculations show that, if the difference in perpendicular distances from a point on the hypotenuse to the two surfaces is ΔZ , the translation of the paraxial focus position is $\Delta Z n_{BS}^{-1}$, where n_{BS} is the index of refraction of the beam splitter cube, and the longitudinal spherical aberration for a ray at N.A. = 0.2 is $7.6 \times 10^{-3} \Delta Z$. The white light fringe plane is translated by $(n_{BS} - n_{BS}^{-1})\Delta Z$ from the actual paraxial focus and the magnification error is $\Delta Z (n_{BS} t)^{-1}$ where t is the total optical length between the object plane and the conjugator medium. The beam splitters that we had obtained had an asymmetry of $\Delta Z = 610 \mu$, which implied unacceptable values for the spherical aberration, magnification and paraxial focus displacement. To correct the aberration as much as possible, we added a fused silica compensator plate of thickness 595 μ between the wafer and beam splitter, as shown in Fig. 1. With this compensator, we found that the white light fringe plane was deviated by 34 μ from the focal plane, which implies that the remaining optical asymmetry is $\Delta Z = 40 \mu$. The uncorrected longitudinal spherical aberration at N.A. = 0.2 is then 0.3 μ, the magnification error expected is $\Delta M = 4 \times 10^{-4}$, and the transverse spherical aberration (which might limit the resolution) is 0.05 μ.

The medium producing the conjugate wave was a solution of Rhodamine 6G perchlorate in acetone. This medium shows virtually no saturation of the absorption at the wave-

length and intensity levels of this experiment and produces the conjugate wavefront by means of forced Rayleigh scattering.⁵ The low thermal conductivity of acetone and the large thermal coefficient of the refractive index make this solvent ideal for image protection experiments. Rhodamine was chosen as the absorber, because it proved photochemically stable and does not fluoresce at a wavelength that exposes photoresist. The concentration was chosen to attenuate the forward pump beam by a factor of 2, near the optimum for this sort of wavefront conjugation. The dye solution was flowed through the 1.8 cm × 0.9 cm cross-section cell at 2 gallons per min in order to suppress long-lived thermal gradients which are detrimental to image quality. Mie scattering from suspended particulates could potentially cause unwanted exposure of the resist. Mie scattering was suppressed by carefully filtering the fresh solution through filters with 0.2- μ pore size and by incorporating a cartridge filter in the dye flow circuit. Ethylene propylene and teflon seals were required throughout the flow system to avoid chemical attack which could liberate particulates.

The conjugate wave transmitted through the beam splitter and compensator plate, focusing to an image on a photoresist film coated on a 1-in. diam borosilicate glass substrate. The substrate was positioned less than 1 mm from the compensator plate and could be tilted and translated in two directions. Rough focusing was accomplished by observing the white light fringes formed in the interferometer consisting of the mask and substrate wafer and the beam splitter cube.² The substrate was then translated 35 μ away from the beam splitter by means of a differential micrometer to the plane of best focus.

Light passing through the resist and substrate was collected by an optical system, which separated the ultraviolet conjugate beam from the visible fluorescence produced by the Rhodamine dye. Part of the conjugate beam was reimaged upon a PIN photodiode, the pulses from which were integrated and their areas summed digitally to yield a measure of total resist exposure. Another portion was imaged upon a fluorescence converter consisting of thin layer of sodium fluorescein dissolved in glycerol and gelatine.⁶ The fluorescent image, thus produced, could be viewed through a magnifier for real-time diagnostics on image brightness and illumination uniformity.

The complex geometry of this system makes it difficult to exactly calculate the expected resolution. The ray diagram in Fig. 3 illustrates the difficulties, as well as techniques yielding approximate estimates. The central ray of the diffraction pattern from the mask is shown as line OBL. The region of the cell illuminated by the pump beam is shown as white, while the unpumped regions of the cell are gray. The image of the object point O is formed at point I. In the cell, ray B-L traverses an unpumped region between the cell wall and point C. In this region, the intensity is attenuated by an amount $e^{-\beta l_u}$ where β is the Beers law absorption constant, and l_u is the arc length through unpumped dye. The ray crosses the pump region between points C and C', and it is in this region that the conjugate wave is generated. The intensity of the conjugate ray at point C can be calculated

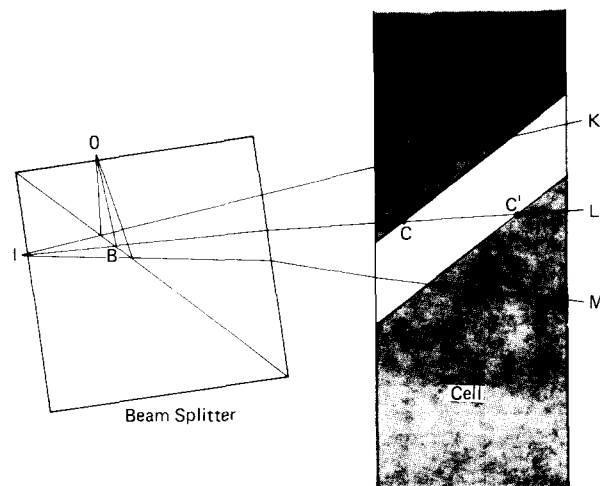


FIG. 3. Ray diagram for estimating the resolution of the projection apparatus. Point O is an object point on the mask which is managed by the apparatus at point I. Ray OBL corresponds to the central ray from point O while rays OK and OM define the effective numerical aperture. The unshaded region of the cell is illuminated strongly by the counterpropagating pump beams and is thus the active region for wavefront conjugation. The line segment C-C' of the central ray interacts with the pump beams and the brightness of the returning ray is proportional to the square of the length of this segment.

ed by solving the appropriate differential equation,⁸ but since the length of the segment C-C' is less than β^{-1} , it is not too bad an approximation to ignore absorption. In the absence of absorption, the intensity of the conjugate ray at point C is proportional to the square of the length of the segment. The conjugate ray must then traverse an unpumped region of the cell where it is attenuated as was the object beam.

The result of these calculations is that the intensity of the conjugate ray corresponding to any of rays in the initial diffraction pattern is proportional to $I \propto e^{-2\beta l_u} l_p^2$ where l_p is the length of the ray segment crossing the pump beam, and l_u is the length of the ray through unpumped dye. Using the diagram in Fig. 3, we were able to plot the intensities of the conjugate rays as a function of diffraction angle θ . The three rays indicated in Fig. 3 are highlighted in the result of this calculation in Fig. 4. Following Hubbard,⁷ we can estimate the effective numerical aperture of this system by noting the angle where the intensity of the returning ray falls to 1/4 of that of the central ray. The corresponding amplitude of the conjugate wave is 1/2 of the initial amplitude. For a sinusoidal input intensity pattern with 100% contrast and spatial frequency at this cutoff, this image would show 60% contrast. As can be seen from Fig. 4, the cutoff angle defined in this way is $\sin^{-1}0.19 = 11^\circ$, implying an effective numerical aperture of N.A. = 0.19 and a maximum useful spatial frequency of N.A./ $\lambda = 535$ lines/mm for normal illumination. If the illumination were altered so that the central ray grazed the edge of the effective aperture, the maximum spatial frequency would increase to roughly 1070 lines/mm.

The situation is simpler in the vertical plane. The pump beam then subtends an angle of 7.8° at the image point, im-

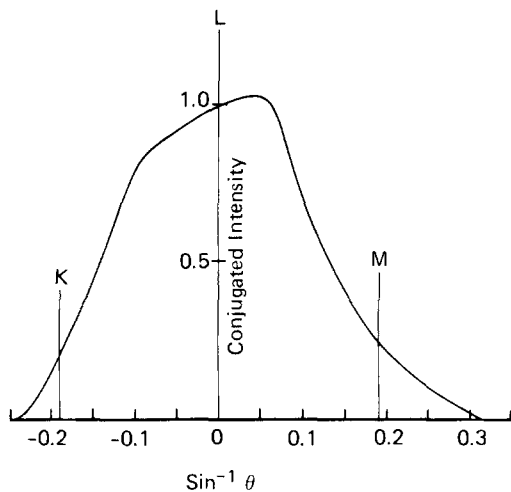


FIG. 4. Calculated relative brightness of returning phase conjugate rays as a function of the diffraction angle at the mask. Zero angle corresponds to the central ray OBL-LBI, while the extreme rays OK-KI and OM-MI are also indicated. The effective numerical aperture of this device is estimated as the arc sine of the angle at which the relative conjugation efficiency falls to 0.25.

plying an effective numerical aperture of 0.068 and a cutoff spatial frequency of 191 line/mm. This limited resolution in the vertical direction is a direct result of the low power of our laser source. Had we stretched the pump beam vertically to improve resolution, we would have sacrificed image brightness (which is proportional to the square of the pump intensity) and unduly lengthened the exposure time necessary to pattern photoresist.

The pulse lengths and beam angles in this experiment allow the expected brightness of the image formed by conjugate wavefront generation to be estimated by the thermal diffusion model of forced Rayleigh scattering.⁴ The relevant parameters appear in Table I. The path length through pumped dye is assumed equal to that of the central ray OBL in Fig. 3. After accounting for the reflection loss in the beam splitter the estimate average image intensity is 52 mW/cm². The photoresists employed require a nominal energy deposition of 100 mJ/cm² for optimal development. Thus, our esti-

TABLE I. Parameters of acetone-rhodamine 6G conjugator experiment.

Heat capacity		
ρC_p	1.71	J/cm ³ °C
Thermal conductivity		
κ	1.79×10^{-3}	W/cm °C
Index of refraction		
n	1.36	
Temperature dependence of n		
$(\partial n / \partial T)_p$	-53×10^{-5}	(°C) ⁻¹
Absorption constant		
β	0.39	cm ⁻¹
Scattering wave vector		
q	1.5×10^5	cm ⁻¹
Grating decay time		
τ_q	2.4×10^{-7}	sec

mated image brightness would imply an exposure time of 1.9 sec.

The theoretical image brightness cannot be achieved in these experiments, because the strict phase matching condition makes it impossible to utilize all of the pump laser power. The theoretical calculation assumes that the pump laser beams are plane waves, or at worst, TEM₀₀ laser modes. Our beams were well collimated, but showed intensity variations across their profiles in the near field, as well as subsidiary maxima of intensity in the far field. Only 60% of the laser harmonic could be focused through at 150- μ -diam spatial filter while the expected diameter of a focused TEM₀₀ with the same diameter at the lens was 32 μ . This fact implied that a significant fraction of the spatially filtered beam propagated at angles larger than the diffraction limit with respect to the beam axis.

Two problems introduced by these aberrant rays are illustrated in the wave-vector matching diagrams in Fig. 5. The upper diagram shows the wave-vector \mathbf{q} of the transient thermal grating formed by the object beam \mathbf{k}_0 and forward pump \mathbf{k}_1 . If the wave vector of the backwards propagating pump \mathbf{k}_2 deviates by an amount $\delta \mathbf{k}$ from the correct phase matching direction in the horizontal plane, a wave-vector mismatch $\Delta K = \delta k \sin \phi$ is introduced. If $\Delta K l_p > \pi/2$ the image brightness is strongly suppressed. A large proportion of the power in the pump beams corresponded to rays that

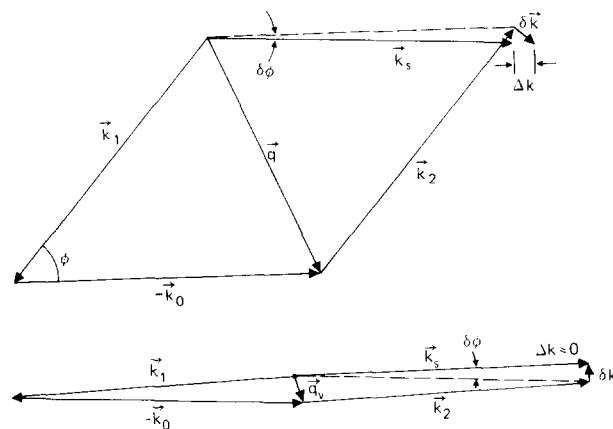


FIG. 5. Wave-vector matching diagrams showing the effects of vertical and horizontal misalignment of the counterpropagating pump beam. The wave-vector of the object ray is labelled \mathbf{k}_0 with the pump waves labelled by \mathbf{k}_1 and \mathbf{k}_2 . The wavevector of the thermal grating written in the medium is \mathbf{q} and the output wave vector is \mathbf{k} . A small misalignment of the counterpropagating pump by an amount $\delta \mathbf{k}$ causes the direction of optimum phase matching for the output wave to shift by an angle $\delta \phi$ and introduces a net mismatch at optimum of Δk . When the pump and object beams propagate at a large angle in the plane defined by \mathbf{k}_2 and $\delta \mathbf{k}$ as at top, the phase mismatch causes the image brightness to drop markedly even for relatively small misalignments. When the pump and object beams propagate at a small angle when projected into the plane defined by \mathbf{k}_2 and $\delta \mathbf{k}$, the phase mismatch is not large enough to suppress the image brightness and the net effect is a displacement of the image. In the geometry of our system the condition diagrammed at top occurs in a horizontal plane and that diagrammed below in the vertical plane. Since the pump beams contain a distribution of wave vectors around the central ray, these effects can blur horizontally oriented features and require critical alignment to avoid modulation of the image brightness by output waves generated by different pump wave vectors.

could thus not be simultaneously phase matched. From previous experiments, we expected the actual image brightness to be five times less than the theoretical value calculated above.⁵ Thus, the expected time required to optimally expose photoresist was roughly 10 sec. The temporal mode structure of the laser fluctuated a bit, however, and vibrations and other effects caused the image brightness to fluctuate. The result was that optimum brightness could not be achieved on each laser shot, and the average brightness tended to be less than that predicted. When the laser system operated poorly, the time necessary to deposit energy sufficient to cause proper resist development was many times longer than predicted.

The lower diagram in Fig. 5 shows an even more serious problem. Pump beam rays propagating away from the axis in a vertical plane do phase match for a wide variety of transverse wave-vectors δk . The image waves thus produce propagate in various directions and cause the image to blur. In the vertical direction the numerical aperture of our system was not sufficient to observe this effect, but a related one was readily apparent. When phase matching is noncritical and the pump beams are not exactly phase conjugates of one another, the intensity at the image will be modulated by interference effects between light scattered from different spatial components of the pump beams. This effect appears as bright and dark horizontal fringes in the image. The period of these fringes depends upon the vertical misalignment of the backwards pump beam and could be used to optimize phase matching for the central ray. At optimum, the entire image was illuminated with maximum uniformity.

MAKING EXPOSURES

The first stage in the preparation of photoresist coated wafers was the careful cleaning of the borosilicate glass substrates. After washing in acetone and ultrasonic cleaning, the substrates were soaked in aqua regia, washed with deionized water and baked dry. An adhesion promoter—hexamethyl disilazane—was then applied and spun off. The var-

ious photoresists listed in Table II were spun on with the desired thickness. The substrates were then baked for 20 min at 90 °C and transferred to the exposure tool.

The wafers were levelled by overlapping the reflections of a helium neon laser alignment beam that was incident upon the mask and wafer through the beam splitter and conjugator cell. With the beam expanded, interference fringes formed in the Michelson interferometer allowed a levelling precision of 0.3μ . The substrate was then translated on its micrometer stage until the white light fringes appeared and further translated to the desired focal plane with a differential micrometer. Up to nine chip exposures could be made on a wafer, and this interferometric focusing procedure was repeated before each exposure.

Thermal effects in the laser and harmonic generation crystals required that the laser warm up for several minutes before a wafer exposure and run continuously during the exposure, even when the wafer was being moved, aligned, etc. A moveable beam stop was inserted to block the entire beam, and a shutter system was employed to block the illuminating beam and thus prevent exposure of the wafer. In operation, the pump beams were unblocked and the exposure meter zeroed. Then the illuminating beam shutter was opened and closed when a predetermined exposure level had been recorded. Typically, a rough focus exposure matrix was run using the first wafer of a given day, with later wafers exposed under more nearly optimum conditions. The time required for each exposure was also recorded. In order to make the image illumination uniform, the illuminating beam was translated back and forth across the mask during each exposure. The effects of illuminating beam displacement could be monitored with the fluorescence converter and also by an oscilloscope displaying the exposure meter photodiode output. A variable illumination geometry simulates some of the effect of incoherent illumination, reducing speckle and averaging out diffraction fringes in the image.

The exposed wafers were developed using the developer solutions recorded in Table II. The end points of develop-

TABLE II. Resist and processing parameters.

Resist	Thickness	Developer	Dilution	Exposure time	Result
AZ2400	1.2μ	AZ2401	4.5:1	65 sec	$1 \times 1 \mu$ Develops properly
AZ2400DUV	0.95μ	AZ2401	4.5:1	35 sec	$0.5 \times 1 \mu$ Develops properly
AZ1370	2.0μ	AZ351	5:1	60 sec	Lift-off problems
AZ1350B	0.5μ	AZ351	5:1	30 sec	$0.5 \times 1 \mu$ o.k., Lift-off for long development
AZ1470	0.8μ	AZ	3:1	100 sec	$0.5 \times 0.75 \mu$ o.k., Lift-off problem

ment were determined using a light microscope and varied somewhat with exposure and other variables. Resist adhesion was a major problem throughout the experiment. Lightly exposed resist films would break up and float off the substrate well before any exposed features developed through the entire film. Thin walls on more highly exposed films also tended to break off once the exposed regions on either side reached the substrate. Even on our best samples, electron microscopy revealed undercut "caves" in the cliffs formed by undeveloped walls of resist. These "caves" appeared to result from preferential dissolution of resist above contamination sites on the substrates. Processing photoresist for sub-micron structures appears to remain an art, especially when the substrate is glass.

Promising developed wafers were sputter coated with 200 Å of palladium gold and inspected using a Hitachi S-500 scanning electron microscope. New and used masks were also inspected to document the effects of laser illumination. Emphasis was on structures showing a spatial resolution of 500 lines/mm and above—that is upon submicron lines and gaps which most strongly test the resolution of a projection system.

RESULTS

Figure 6 shows the image of one of our resolution test chips. The test pattern on the mask consisted of a checkerboard pattern with five transparent lines within each opaque square. The linewidths varied from 2 to 0.5 μ nominal and the gaps between lines varied from 4 to 0.5 μ nominal. The

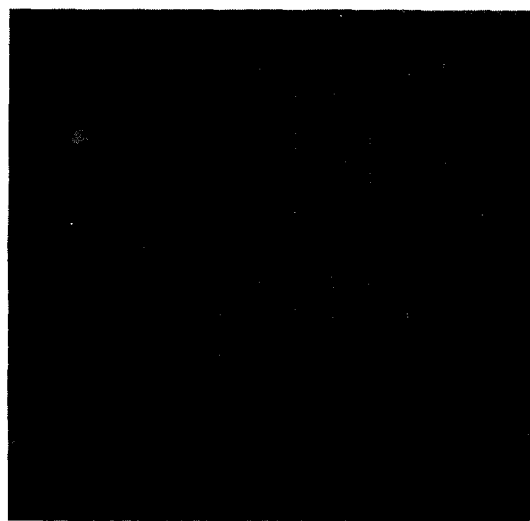


FIG. 6. A scanning electron micrograph of the developed resist pattern produced by the image of our resolution test chip as projected by wavefront conjugation. The pattern shown here was produced in a 0.95- μ -thick layer of AZ1370 resist in a 35-sec exposure and appears overdeveloped after 2 min in 5:1 diluted AZ351 developer solution. The top row contains the largest transparent lines—2 μ wide nominal—with the maximum spacing of 4 μ at left. The spacings or gap between lines decreased from left to right while the linewidths decreased from the top towards the bottom. From top to bottom the linewidths are 2, 1.5, 1.0, 0.75, 0.5, and 0.0 μ , while the gap widths are from left to right 4, 2, 1, 0.75, 0.5, and 0.0 μ nominal.

masks were prepared by vector scanned electron beam lithography and turned out to be slightly overdeveloped with wider lines than nominal and narrower gaps between lines. Nevertheless, the pitch of the five line patterns remained correct. The chip shown in Fig. 6 was exposed in 35 sec in 0.95 μ of AZ1320 photoresist. The minimum exposure times required to cause each resist to develop through to the substrate is recorded in Table II. Proper development was judged on 1- μ linewidths. Larger structures, of course, developed more readily.

Figure 7 shows some nominal 1- μ lines and gaps in AZ-2400DUV which were somewhat overexposed in 36 sec. Perhaps the best combination of resolution and exposure time was achieved using AZ1470 resist. Typical electron micrographs appear in Figs. 8 and 9. The best resolution achieved using this tool is shown in Fig. 8 (800 lines/mm). The exposure time required was 99 sec, and the development time was reduced to eliminate liftoff. (Off axis illumination was employed to increase resolution during this exposure.) In viewing these scanning electron micrographs one should note the absence of speckle, which results from the low level of light scattered from dust on surfaces and the brightness of the images projected.

Figure 10 illustrates some of the effects of misalignment and stray wave vectors in the pump beams. Figure 10(a) shows a pattern of 2- μ lines with 2- μ gaps exposed with a properly aligned backwards pump beam. Figure 10(b) shows the result of changing the vertical alignment slightly in the middle of the exposure. Since the total energy deposited re-

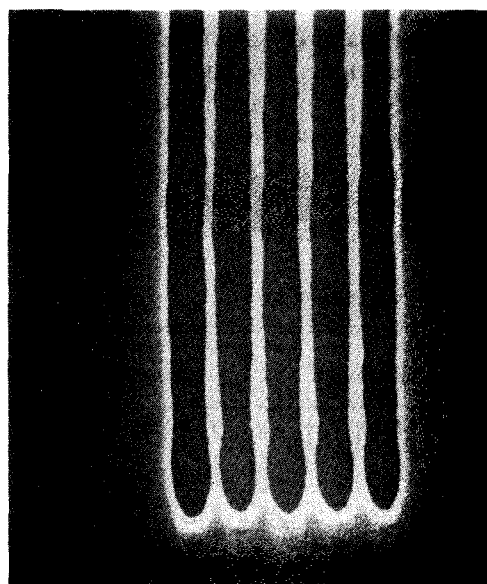
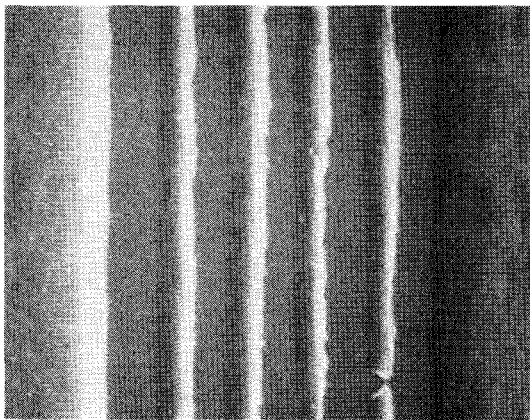
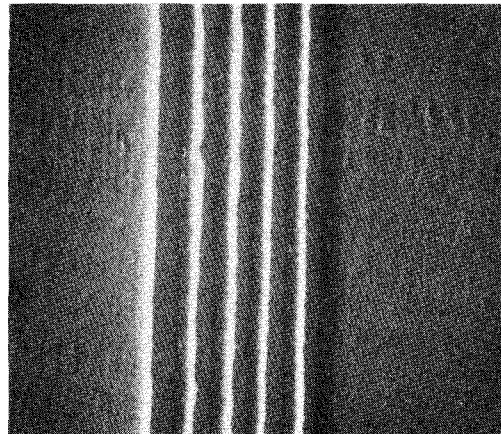


FIG. 7. Tips of five 1.0- μ nominal lines with 1.0- μ nominal gaps as patterned in 0.9 μ of AZ2400DUV resist. The exposure time was 36 sec, and the development time was 1 min in 4.5:1 diluted AZ2401 developer. The thin undeveloped walls reflect the fact that the gaps on our mask were narrower than nominal. Nevertheless, this pattern is overexposed. It does demonstrate, however, that a 500 line pair per millimeter spatial frequency can be projected by our system.



5 μ

FIG. 8. Our highest resolution image—a pattern of five 0.5- μ nominal width lines with 0.75 nominal width gaps imaged on 0.8- μ -thick AZ1470 resist. The resolution thus demonstrated is 800 line pairs/mm. Off axis illumination was required for this resolution, and the necessary exposure time was 99 sec. Clear evidence of undercutting of some of the walls as a result of substrate contamination can be seen at center right. Liftoff as the result of such undercutting was a persistent problem.



5 μ

FIG. 9. Developed resist image of a pattern of 0.5- μ nominal lines with 1.0- μ nominal gaps in AZ1470. The exposure and development conditions were similar to Fig. 8, but the somewhat thicker walls were less sensitive to undercutting. This 667 line pairs/mm resolution could be achieved with only slightly oblique illumination.

mains constant, the result is two underexposed images translated from one another. The appearance of two images reflects the weak phase-matching condition in the vertical plane. Figure 10(c) shows the same pattern when the back mirror is tilted in a horizontal plane in the middle of an exposure. The main result of this misalignment is to make the image weaker, and the time required for proper exposure longer. The strict phase matching condition prevents degradation of the image.

All the patterns in Figs. 6–10 were obtained with the narrow lines vertical, thus orienting the diffraction patterns of the finest features to take maximum advantage of the large numerical aperture in the horizontal plane. When the mask was rotated 90°, the best resolution attainable was 160 lines per millimeter or a 3- μ line with 3- μ gap. This is completely consistent with the geometrical 0.068 numerical aperture in the vertical plane.

Figure 11 shows some degradation resulting from continued laser illumination of a mask. There appear to be a number of effects which degrade a mask subject to intense pulsed laser light incident from the glass side of the chromium layer. Most dramatically, the chromium film seems to lift off the glass, often without other damage. Through a microscope, the main evidence of liftoff is that the opaque lines between the apertures appear to undulate and can no longer be simultaneously focused. Even when the chrome film does not lift off, it appears that laser illumination widens the apertures etched in the film and reduces the width of opaque lines. The film in some areas appears to have been thinned, thus becoming more transparent. Often the thinned regions show diffraction patterns characteristic of laser light scattered from dust particles on the back surface of the mask. Finally, at high intensity, the chromium film can be made to crack and peel off over areas of several square microns. All of these effects degrade the image quality. Many times, we

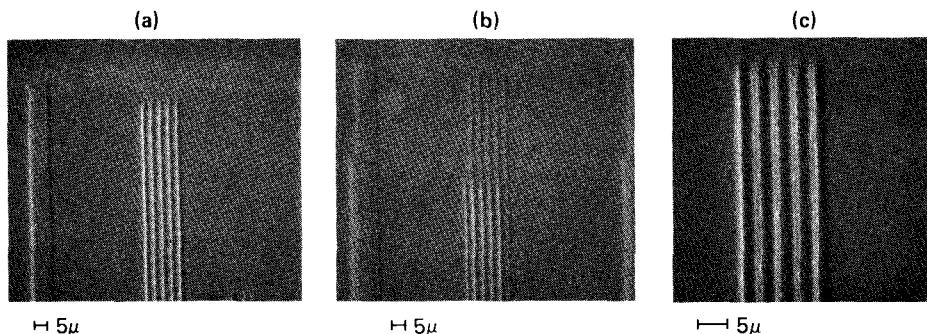


FIG. 10. Some effects of pump beam misalignment on the image. (a) shows a pattern of 2- μ lines and gaps exposed with a properly aligned counterpropagating pump. (b) shows the effect of altering the direction of the pump by tipping the retroreflector mirror around a horizontal axis in the middle of an exposure. Two underexposed images result, translated vertically with respect to one another. (c) shows the absence of any effect on image quality when the retroreflector mirror is rotated around a vertical axis. The more stringent phase matching condition in the horizontal plane does reduce image brightness and thus lengthens the time necessary to reach a present exposure level by about a factor of 3.

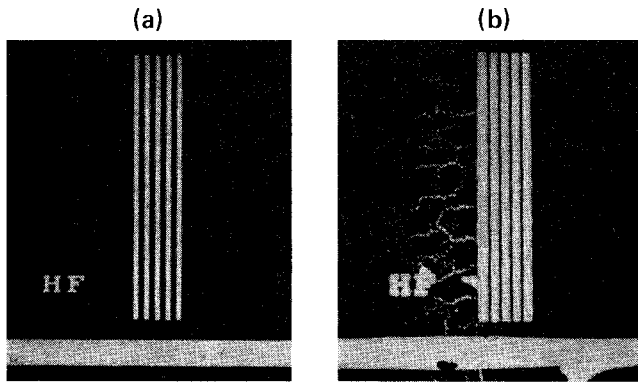


FIG. 11. Light micrographs of portions of a new and a used mask pattern. Both figures show $2\text{-}\mu$ nominal lines with $2\text{-}\mu$ nominal gaps, but the used mask in (b) shows a variety of damage. The opaque gaps are thinner than nominal, and the chromium film has lifted off the glass mask substrate in several places. The film in the opaque region to the left of the five-line pattern shows cracks and lines of pinholes. Such mask damage appears after less than 1 h of illumination at peak laser intensities of 2 MW/cm^2 .

found that mysterious reductions in image quality were related to subtle—and not so subtle—mask damage.

Our experience indicates that conventional chrome on glass masks will deteriorate after less than an hour of illumination by a pulsed laser with peak intensity levels of 2 MW/cm^2 and average intensities of 210 mW/cm^2 . No other optical element in the phase conjugation exposure system damaged at such low power levels. Conventional aluminum mirrors can survive such treatment, even when the light is incident on the aluminum through the glass substrate. Chromium masks without etched apertures also proved more resistant. In degenerate four-wave mixing, the image brightness is proportional to the product of the illuminating beam intensity and the intensities of the two pump beams. If mask damage limits the illuminating beam intensity, it may not be possible to significantly shorten the exposure times below that achieved here.

In spite of repeated efforts, we were unable to reduce the exposure time necessary to induce development through the resist film below 30 sec for a 0.28-cm^2 area. In fact, our best resolution was achieved with exposure times above 90 sec for a 0.3-cm^2 illuminated mask area, but this larger number may

reflect recurrent problems with liftoff due to wafer cleaning and processing difficulties. Exposures shorter than about 15 sec typically reached an end point in which clear surface development could be seen, but in which residue several tenths of a micron thick remained even in the largest developed areas. Our interpretation of this phenomenon is that the $3550\text{-}\text{\AA}$ light employed could not bleach through the absorbing molecules in the top of the resist film, and left the lower portion of the resist essentially unexposed. Also, pulsed laser exposure of resist has been shown to require roughly a factor of three more energy deposition for development comparable to ordinary lamp exposure.¹⁰ In wavefront conjugation lithography where the image brightness is not very high, this factor of three can be prohibitive.

PROPOSALS FOR A PRACTICAL CAMERA

If a practical wavefront conjugation lithography system is ever to be developed, it will be based on a laser system that can produce high average power, high peak power, and an output beam that is essentially TEM_{00} . Given such a laser, wavefront conjugation by forced Rayleigh scattering can project images with sufficient brightness and resolution to supersede other optical technologies. No suitable laser has, however, yet been designed.

Figure 12 illustrates how such a system might be configured. The laser sources would be ultraviolet rare gas halide lasers, similar to those presently being developed for other large scale optics applications. The system would incorporate a small oscillator producing a single transverse mode output with a linewidth small enough to insure a coherence length greater than 20 cm. Such laser oscillators can be built using a microwave sustained laser discharge.⁷ The output of the oscillator is then stretched, collimated, and spatially filtered into the profile desired for the pump beams and directed into a nonreciprocal beam splitter. This device would incorporate polarization selective optics and a Faraday rotator or quarter wave plate in order to direct the majority of the oscillator output into the amplifier while directing the amplifier output into the conjugator medium. Large discharge pumped laser amplifiers distort wavefronts, introducing aberrations, but a stimulated Brillouin scattering wavefront

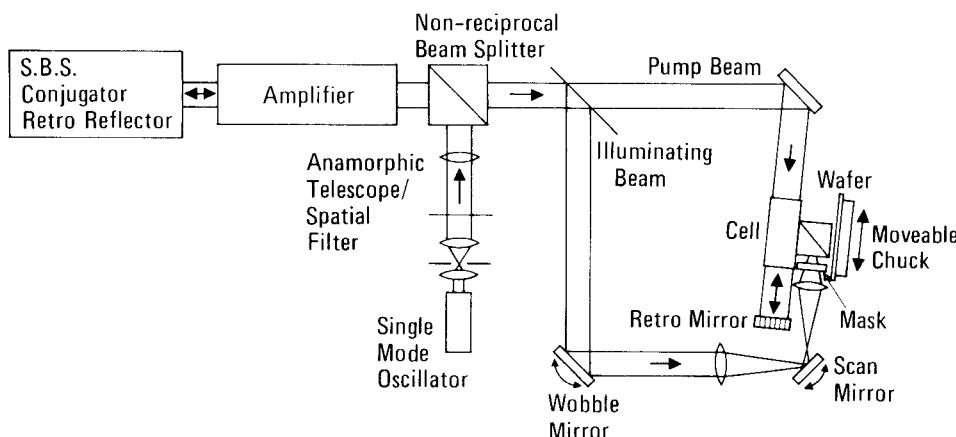


FIG. 12. A conceptual design for a $1\times$ step and repeat exposure camera based upon phase conjugate wavefront generation by forced Rayleigh scattering. The essential element is a laser capable of both high average power and TEM_{00} beam quality. The output of the laser would be split into a pump beam and an illuminating beam which could be scanned in position and wobbled in angle of incidence upon the mask. A 90° geometry would be employed to maximize the numerical aperture. The dye would flow through the cell vertically. For a 25-mm -square field, the size of the beam splitter cube would be 85 mm .

conjugator has been shown capable of reflecting 95% of the incident radiation.⁹ The reflected beam propagates back through the amplifier, having its aberrations corrected as its power increases. The output of this laser system is then split into a pump and illuminating beam. The power in the illuminating beam would be kept low enough to prevent mask damage, while the pump power would be great enough to insure high efficiency conjugation over a significant aperture size.

If such a diffraction limited laser system can be engineered, the theoretically predicted wavefront conjugation efficiencies can be achieved. For a 50% reflection efficiency at the conjugator (roughly 12% of the light transmitted through the mask would be incident on the wafer unless a polarization selective beam splitter were employed) and a 25-mm-square useable field at N.A. = 0.5, the peak pump power required by the acetone/rhodamine conjugator would be 850 MW. At a repetition rate of 100 pps, this implies an average laser power of 1.7 kW for the 20-ns pulse width typical of rare gas halide systems. If the peak illuminating beam intensity were to remain at the 2 MW/cm² level of the current experiments, the time required to expose a 25-mm-square chip would be 0.2 sec.

The beam splitter cube necessary for such a chip size would be 85 mm on a side, while the aperture of the conjugator medium would be 150 mm square. At present, the absorbing liquids used for forced Rayleigh scattering are the most efficient phase conjugation media available in such large area samples. Crystalline photorefractive media can be more efficient, but do not project images of sufficient brightness and at present cannot be grown as large uniform boules. The pump window would be 85 × 150 mm implying a maximum pump intensity of 10.4 MW/cm² for acetone/rhodamine solution. In such a system, it is important to design the condenser optics in the illumination beam path to direct the central ray everywhere on the mask towards the center of the pumped region of the conjugator. To reduce residual illumination nonuniformities and to simulate reduced partial coherence, both the position of the illuminating beam and its angle at the mask should be varied. Shown in Fig. 12 are two rotatable mirrors, a wobble mirror which is imaged by the condenser onto the mask plane, and a scan mirror imaged into the conjugator cell. Rotating the wobble mirror alters the angle of illumination at the mask, while rotating the scan mirror alters the position of the illuminating beam.

The system shown would function as a 1 × step and repeat camera with the wafer in its chuck moving past the image projected by the beam splitter cube. The mask and cube would be smaller than the wafer. Careful engineering would be required to maintain adequate clearance for the wafer, while providing optical paths for the pump and illuminating beams, mechanical support for the optics and shielding from unwanted reflections. Our experimental tool

indicates that these considerations can be fulfilled.

The conjugator shown in Fig. 12 employs the 90° geometry to maximize the numerical aperture. The laser must then have sufficient power and mode quality to overcome the lowered efficiency. Focusing and alignment could be achieved either conventionally or interferometrically, as discussed in previous sections. It is clear that engineering an adequate prototype projection camera is a major—but possibly worthwhile—undertaking, at the limit of the present state of the art of laser engineering and coherent optics. With a 249-mm laser source, the 0.5 numerical aperture implies a limiting resolution of 2000-lines/mm, 0.25-μ features. The depth of focus would be roughly ± 0.22 μ.

CONCLUSION

In summary, we have shown that images with a resolution of 800 line pairs per millimeter can be projected by phase conjugate wavefront generation by forced Rayleigh scattering. The resolution achieved is as predicted by theory at the numerical aperture of our device with oblique illumination. The time required to expose photoresist is longer than expected: 30 sec per 0.3 cm² for 500 liter/mm resolution and 100 sec per 0.3 cm² at submicron resolution. The increased exposure time results partly from a decrease in image brightness reflecting the low quality of the pump beam and partly from a decrease in resist sensitivity when pulsed illumination is employed. Speckle and spurious exposure is absent even though a liquid medium has been employed as the conjugator. Difficulties with mask damage and damage to cemented optics were encountered at power levels lower than predicted. Raising the image brightness, therefore, can only be accomplished by improving the pump beam quality and power and not simply by increasing the mask illumination. Engineering a plausible projection camera appears to be a major undertaking, requiring the development of a specialized pump laser. Such a program might ultimately be justified by the need for a deep UV or vacuum UV projection camera, but at present does not seem advisable.

¹M. D. Levenson, *Opt. Lett.* **5**, 182 (1980).

²M. D. Levenson, K. M. Johnson, V. C. Hanchett, and K. Chiang, *J. Opt. Soc. Am.* **71**, 737 (1981).

³R. G. Caro and M. C. Gower, *Appl. Phys. Lett.* **39**, 855 (1981).

⁴M. C. Gower and R. G. Caro, *Opt. Lett.* **7**, 162 (1982).

⁵K. Chiang and M. D. Levenson, *Appl. Phys. B* **29**, 23 (1982).

⁶T. M. Hansch, F. Varsanyi, and A. L. Schawlow, *IEEE J. Quantum Electron.* **QE-7**, 45 (1971).

⁷J. Hubbard, *J. Opt. Soc. Am.* **71**, 1029 (1981).

⁸R. C. Desai, M. D. Levenson, and J. A. Barker, *Phys. Rev. A* **27**, 1968–1976 (1983).

⁹M. C. Gower, *Opt. Lett.* **7**, 423 (1982).

¹⁰K. Jain, C. G. Willson, and B. J. Lin, *IEEE Electron Devices Lett.* **3**, 53 (1982).